Chemistry–A European Journal
Research Article
doi.org/10.1002/chem.202104240
Chemistry Europe
European Chemical Societies Publishing
www.chemeurj.org

Combined in Silico and in Vitro Approaches To Uncover the Oxidation and Schiff Base Reaction of Baicalein as an Inhibitor of Amyloid Protein Aggregation

Natércia F. Brás[+],*[a, b] Salavat S. Ashirbaev[+],[b] and Hendrik Zipse[b]

Abstract: The oxidized form of baicalein (**BA**) leads to covalent binding with human amyloid proteins. Such adducts hamper the aggregation and deposition of fibrils. A novel reaction of **BA** with pentylamine (**PA**) as a model for the lysine side chain is described. This is the first study addressing the atomistic details of a Schiff base reaction with the trihydroxylated moiety of **BA**. Nuclear magnetic resonance and mass spectrometry approaches clearly indicate the formation of dehydrobaicalein in solution as well as its condensation with **PA** under aerobic conditions, yielding regioselectively C6-substituted products. The combined results suggest initial ion pair formation between **BA** and **PA**, followed by a redox chain reaction: the initiation by oxygen/air; an *o*-quinone-based chain involving oxidation and reduction steps; and extra off-chain formation of a doubly oxidized product. These mechanistic details support the anti-amyloid activity of **BA** and endorse its trihydroxyphenyl moiety as a pharmacophore for drug-design studies.

Introduction

Human islet amyloid polypeptide (hIAPP, also known as amylin) is a 37-residue neuroendocrine hormone co-expressed and co-secreted with insulin by pancreatic β-cells. Type 2 diabetes (T2D) patients have increased blood concentrations of hIAPP, causing its aggregation and deposition as toxic insoluble fibrils that significantly contribute to cell death.[1] Because of this, the inhibition of hIAPP amyloidosis is an emerging target for the treatment of T2D. However, this is a challenging task due to the complexity of protein self-assembly and the poor knowledge of the molecular details of inhibition, despite the growing number of proposed mechanisms by which a drug can interfere with amyloids.[2]

Many promising natural phenolic compounds have been reported as small inhibitors of protein misfolding and aggregation.[3] The molecular structure of flavonoids enables them to chemically bind to and avoid assembly of the hIAPP fibrils. Epigallocatechin gallate (EGCG), quercetin, myricetin, chrysin and baicalein (Scheme 1a) are some examples of flavonoids with recognized anti-amyloidogenic activity.[4]

Previous studies proposed that these molecules interact with and stabilize the amyloidogenic peptides by covalent and/or noncovalent interactions.[3b] Due to antioxidant properties and the propensity to undergo autoxidation (by enzymatic or nonenzymatic reactions), certain polyphenols can act as electrophiles and interfere with proteins through specific covalent contacts.[3b,5] Indeed, chemical modifications by Schiff base and Michael addition reactions have been reported between nucleophilic amines and thiols of amyloid peptides and electrophilic reactive groups of *o*-quinones and aldehyde molecules.[3b,4a,b,6] It has been proposed that EGCG oxidizes readily in solution and the oxidized forms can produce Schiff base adducts with hIAPP and β-amyloid peptide (Aβ).[7] The inhibitory mechanism of Aβ aggregation by (+)-taxifolin also requires its autoxidation to form an *o*-quinone to react with lysine residues.[8] Also, covalent adduct formation significantly affects anti-aggregation effects of quercetin on α-synuclein.[6a] Recently, a study with tetramers of caffeic acid suggested that the greater the number of catechol moieties, the greater the inhibitory effect on IAPP aggregation.[9]

Baicalein (**BA**, **1**) is a flavone isolated from the roots of the traditional Chinese herbal medicine *Scutellaria baicalensis* known to have plenty of pharmacological activities such as antioxidant, anti-inflammatory and anti-tumor properties[10] as well as anti-amyloid abilities against Aβ,[11] amyloid precursor protein,[12] α-synuclein,[6b] insulin,[13] calcitonin[14] and hIAPP.[4b]

Upon oxidation, **BA** forms several intermediates including the dehydrobaicalein (**DBA**) quinones, which are susceptible to nucleophilic attack through imine (Schiff base) formation by the side chain of Lys residues, leading to covalent modification. Velander et al. identified Schiff base-mediated hIAPP:baicalein

[a] *Dr. N. F. Brás[+]*
LAQV, REQUIMTE
Departamento de Química e Bioquímica
Faculdade de Ciências, Universidade do Porto
Rua do Campo Alegre s/n, 4169-007 Porto (Portugal)
E-mail: nbras@fc.up.pt
natercia.braz@cup.uni-muenchen.de

[b] *Dr. N. F. Brás,[+] S. S. Ashirbaev,[+] Prof. H. Zipse*
Department Chemie
Ludwig-Maximilians-Universität Muenchen
81377 Muenchen (Germany)

[+] *These authors contributed equally to this work.*

Supporting information for this article is available on the WWW under https://doi.org/10.1002/chem.202104240

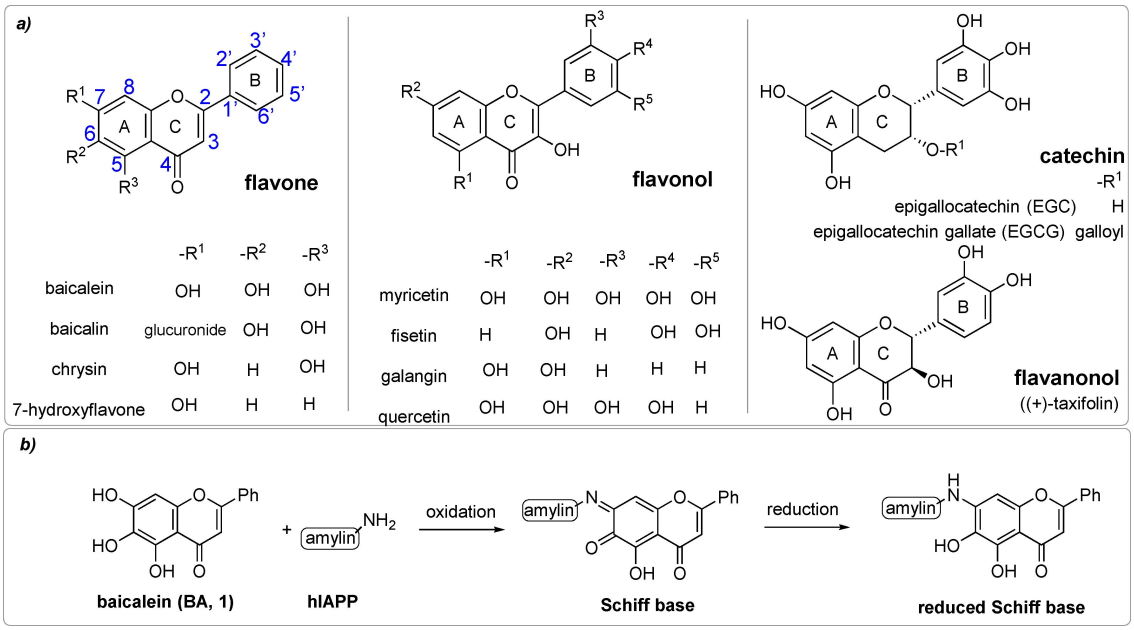

Scheme 1. a) Molecular representations of the flavonoids mentioned in this work. b) The proposed reaction for baicalein–hIAPP conjugation based on mass spectrometric evidence is shown.

adducts by mass spectrometry (Scheme 1b).[4b] They pointed out the importance of vicinal hydroxy groups in the A ring of **BA** (5,6,7-trihydroxyflavone) for its anti-amyloid inhibitory effects;[4b] however, the underlying molecular details of the chemical reaction are not yet fully understood. Zhu et al. also demonstrated that the inhibition of in α-synuclein is very sensitive to the oxidation state of **BA**.[6b] While minor inhibitory effects could be observed under anaerobic conditions, stronger inhibition can only be observed in the presence of oxygen, highlighting the importance of the quinone forms and covalent modifications to prevent amyloid fibril formation. They also concluded that it is the interaction between the oxidized baicalein with both hIAPP and α-synuclein peptides that is responsible for the anti-amyloid activity (instead of the antioxidant potential of **BA**).[6a,b] In addition, other studies pointed out that the amination of pyrogallol derivatives by ammonia/water treatment is a regioselective amino-substitution that proceeds under mild conditions (e.g., presence of molecular oxygen) without a catalyst.[15]

Due to the occurrence of Schiff bases as transient intermediates in catalysis, chemical engineering and medicine, the nucleophilic attack of primary amines on quinones and aldehyde moieties is well studied in the literature.[16] In general, it involves the formation of a carbinolamine, followed by a dehydration reaction that forms an imine. However, as the mechanistic pathways can depend on the intermediate species and environmental conditions such as chains of water molecules that act as proton transporters, this reaction can be far from straightforward.[16c,17]

In addition to the critical role of Lys residues for Schiff base covalent inhibition mechanisms, they also are crucial hot spots for mechanisms involving both hydrophobic and electrostatic interactions such as those present in Lys-specific tweezers.[18] The unique Lys residue present in the hIAPP (the N-terminal residue-Lys1) has not been pointed out as a part of the fibril core structure; however, recent studies proposed that covalent modifications of Lys1 such as glycation and Schiff base reaction can significantly affect the aggregation and the hIAPP-membrane interactions.[19] Therefore, Lys1 of hIAPP also plays a role in inhibitor binding, and the uncovering of its chemical modification with atomistic detail will be very helpful for amyloidosis events. Even though baicalein has been shown to covalently bind the Lys1 of hIAPP, its mechanism of action remains poorly understood.

This study proposes to clarify the atomistic details of the Schiff base reaction between the thermodynamically most favored dehydrobaicalein tautomers and the Lys1 of hIAPP (**DBA**–Lys covalent adduct). For this purpose, combined in silico (quantum mechanical calculations) and in vitro (NMR and HRMS) assays are employed to i) assess the oxidation and ionizable properties of baicalein in solution, and ii) to identify the preferable Schiff base adducts that are formed.

Experimental Section

Computational methods: The geometries of the various tautomeric forms (and respective rotamers) of **BA** and **DBA** were optimized using the hybrid B3LYP[20] density functional associated with the empirical dispersion D3 correction of Grimme et al.,[21] in combination with the 6-31+G(d,p) basis set.[22] The solvent effects were accounted for by the SMD solvation model.[23] Harmonic vibrational frequency calculations were performed at the same level of theory to obtain the thermochemical corrections to the enthalpic and free

energies at 298.15 K. The charge distribution was analyzed by applying the NBO formalism.[24]

To analyze the free energy of the various tautomeric forms of the reaction products, the potential energy surface (PES) of the interaction between a Lys side chain and each tautomer of dehydrobaicalein was explored by a linear transit scan along the dihedral angle that governs that N–C bond (a representative calculation is displayed in Figure S1 in the Supporting Information). Then, the enthalpic and free energies were obtained by optimization without constraints by using the same level of theory (SMD(water)/B3LYP-D3/6-31 + G(d,p)).

The binding mode between the most stable tautomeric forms of **DBA** and the Lys1 of hIAPP (PDBID 2KB8) was obtained by molecular modelling and molecular dynamics (MD) simulations. Throughout the MD simulations, a constant force was used to restrain the *o*-quinone ring of **DBA** close to the amine side-chain of Lys1. The details of the MD procedure are provided in the Supporting Information. The prevalent conformations for each hIAPP:dehydrobaicalein complex obtained from clustering analysis revealed that the interaction between the side chain of Lys1 and the flavonoid is isolated from the remaining peptide residues (Figure S2). Because of this, and to directly compare with the current experiments, a reduced model system including **DBA**, 1-pentylamine as a mimic of the Lys1 side chain, and one water molecule was then used to explore the chemical reaction pathways. The truncated Lys1 residue is hereinafter referred to as pentylamine (**3**, **PA**) for simplicity. This molecule is an excellent model to represent the lysine side chain due to the great similarity of their experimental pK_a values (10.6[25] and 10.5–10.7[26] for **PA** and Lys, respectively). Previous studies also used truncated lysine models such as 1-butylamine, which also has a pK_a of 10.6, to represent this amino acid.[27] Indeed, the use of aliphatic primary amines is often used to represent lysine residues in reaction mechanism studies using quantum chemical and/or quantum mechanics/molecular mechanics methods.[6c,27b,28] Herein, the **PA** was used to maintain the topology from the alpha carbon atom which better characterizes the complete lysine side chain.

The geometries of reactants, transition states, intermediates and products were optimized at the B3LYP-D3/6-31 + G(d,p) level of theory in conjunction with the SMD model. The reaction pathways were followed from the transition states to both the reactants and the products by using the intrinsic reaction coordinate (IRC) method. The nature of the stationary points was confirmed by calculating vibrational nuclear frequencies at the same level of theory. Thermochemical corrections to the free energies at 298.15 K were considered. Single-point energy calculations were carried out by using the DLPNO-CCSD(T) method combined with the larger cc-pVTZ basis set.[29] The B3LYP calculations were performed by using the Gaussian 09 program package,[30] whilst the DLPNO-CCSD(T) calculations were carried out by using the ORCA program package.[31]

To determine the pK_a values of baicalein, a proton exchange computational approach[32] was employed, using reference flavonoids with known pK_a. Chrysin and galangin (Scheme 1a) were used as reference molecules because the former is structurally similar, whereas the latter has the same number of ionizable groups of baicalein. Equation (1) was used to calculate the free energy for the deprotonation reaction ΔG^*_{sol}, which is then employed in the pK_a determination [Eqs. (2) and (3)].

$$\Delta G^*_{sol} = G_A + G_{ref,H^+} - G_{HA} + G_{ref} \quad (1)$$

$$\Delta pK_a = \frac{1}{2.303\ RT}\ \Delta G_{sol}{}^* \quad (2)$$

$$pK_a(HA) = pK_a(H_{ref}) + \Delta pK_a(HA) \quad (3)$$

Experimental methods: All reactions sensitive to air and moisture were performed under a nitrogen atmosphere and the glassware as well as magnetic stir bars were dried overnight in a dry oven at 110 °C.

Solvents, reagents: All reagents and solvents were purchased from TCI, Sigma-Aldrich or Fisher Scientific. All air- or water-sensitive reagents were stored under nitrogen.

NMR spectroscopy: All ^{1}H NMR spectra were recorded by Bruker 400 in [D$_6$]DMSO at 400 MHz at 23 °C. All ^{13}C NMR spectra were recorded, respectively, at 101 MHz. The chemical shifts are reported in ppm (δ), relative to the resonance of [D$_6$]DMSO at $\delta = 2.50$ ppm for ^{1}H and for ^{13}C{1H} relative to the resonance of [D$_6$]DMSO $\delta =$ 39.52 ppm. Spectra were imported and processed in the MestreNova 14.1.1 program. For ^{1}H NMR spectra the multiplicities (d = doublet, t = triplet, q = quartet, hept = heptet, dd = doublet of doublets, m = multiplet), coupling constants *J*, number of protons and assignment to the structure are reported. In ^{13}C NMR spectra singular carbons are marked with (s).

Mass spectrometry: For electrospray ionization (ESI) spectra a Thermo Finnigan LTQ FT ultra Fourier transform ion cyclotron resonance mass spectrometer was utilized. Atmospheric pressure chemical ionization (APCI) measurements were performed on an Advion CMS instrument using positive ion mode.

Melting point: Melting points were measured on a BUCHI Melting Point M-560.

IR spectroscopy: IR spectra were measured on a PerkinElmer FTIR BX spectrometer mounting an ATR technology module.

UV/VIS spectroscopy: UV/VIS spectra were measured on UV/VIS Varian Cary 50 spectrometer.

More details about the experimental procedures are provided in the Supporting Information.

Deposition Number 2124561 (for the **TAP**–**PA** complex) contains the supplementary crystallographic data for this paper. These data are provided free of charge by the joint Cambridge Crystallographic Data Centre and Fachinformationszentrum Karlsruhe Access Structures service.

Results and Discussion

Due to their chemical structure, phenolic compounds such as **BA** can be oxidized to the respective quinone forms, whose electrophilic character provides the basis for reactions with nucleophiles such as the lysine residues of amyloidogenic proteins. However, different *o*-quinone species can differ in inhibitory activities and act by different mechanisms, suggesting that other properties of the molecules may also be relevant for inhibition. Thus, mechanistic studies with *o*-quinone species have attracted special interest to help optimize *o*-quinone-based drug candidates. Following this idea, in this paper, we assess the atomistic details of the reaction mechanism between several *o*-quinone–baicalein forms and **PA** through quantum chemical calculations. As previously mentioned, the primary

step of the Schiff base reaction between **BA** and **PA** must be the oxidation of the trihydroxylated moiety of **BA**. Therefore, prior to the mechanistic calculations, a deeper understanding of the structure, oxidation and ionization forms of **BA** is performed.

Theoretical analysis of baicalein and dehydrobaicalein (DBA) tautomers

Molecular structures of all possible conformers of **BA** were optimized at the SMD(water)/B3LYP-D3/6-31 + G(d,p) level of theory (Table S1). Energies were subsequently refined through DLPNO-CCSD(T)/cc-pVTZ single point calculations and combined with thermochemical corrections to free energies and solvation energies for water to obtain free energies in water at 298.15 K. The subsequent discussion will focus on these high-level results, if not mentioned otherwise. The geometry with the three hydroxy groups in "anticlockwise" orientations is more stable by 18.5 kJ mol^{-1} than the "clockwise" geometry (Figure S3 and Table S1). This is in agreement with previous results pointing out the "anticlockwise" conformer of **BA**. As the most stable, as it maximizes the number of H-bonds (C7–OH···O–C6 of 2.23 Å, C6–OH···O–C5 of 2.32 Å and C5–OH···O–C4 of 1.71 Å).[33] Baicalein has a slightly nonplanar structure (C2–C1′ length of 1.471 Å and a torsion angle around this bond of 21.0°), which also agrees with previous X-ray and theoretical studies.[33a,34] The conformational energy analysis of **BA** indicates a nonplanar conformation (torsion angle of 22.8°) as the lowest potential energy geometry.[34] Upon oxidation, baicalein can form four different dehydrobaicalein (**DBA**) tautomers (**2a**–**2d**, Scheme 2), each of which comes in two different conformers with respect to the remaining hydroxy group (**2e**–**2h**, Scheme S1 and Table S2a and b). Tautomer **2a** is found to be most stable in an aqueous environment, followed by tautomer **2d** with an energy difference of 7.4 kJ mol^{-1}. This quite small energy difference suggests that both tautomers are populated at ambient temperature. Both molecules are *o*-quinones that are much more stable than the zwitterionic forms **2c**/**2g**. Interestingly, a different anti-amyloid activity is also observed for *o*- and *m*-quinones. The structure-activity relationship analyzed for the inhibition of hIAPP amyloid formation by baicalein and its analogues reveals that both *o*-quinones (5,6-dihydroxyflavone and 6,7-dihydroxyflavone) also have activity, while this is not so for 5,7-dihydroxyflavone.[4b] The presence of vicinal hydroxy groups on the phenyl rings of polyphenolic molecules is also reported as essential for their inhibitory activity against human calcitonin aggregation.[14]

As observed for **1**, both **2a** and **2d** have slightly nonplanar structures (torsion angles around the C2–C1′ bond of 20.2° and 18.3°, respectively). In addition, both tautomers have intramolecular H bonds: in **2a** the C7–OH interacts with the

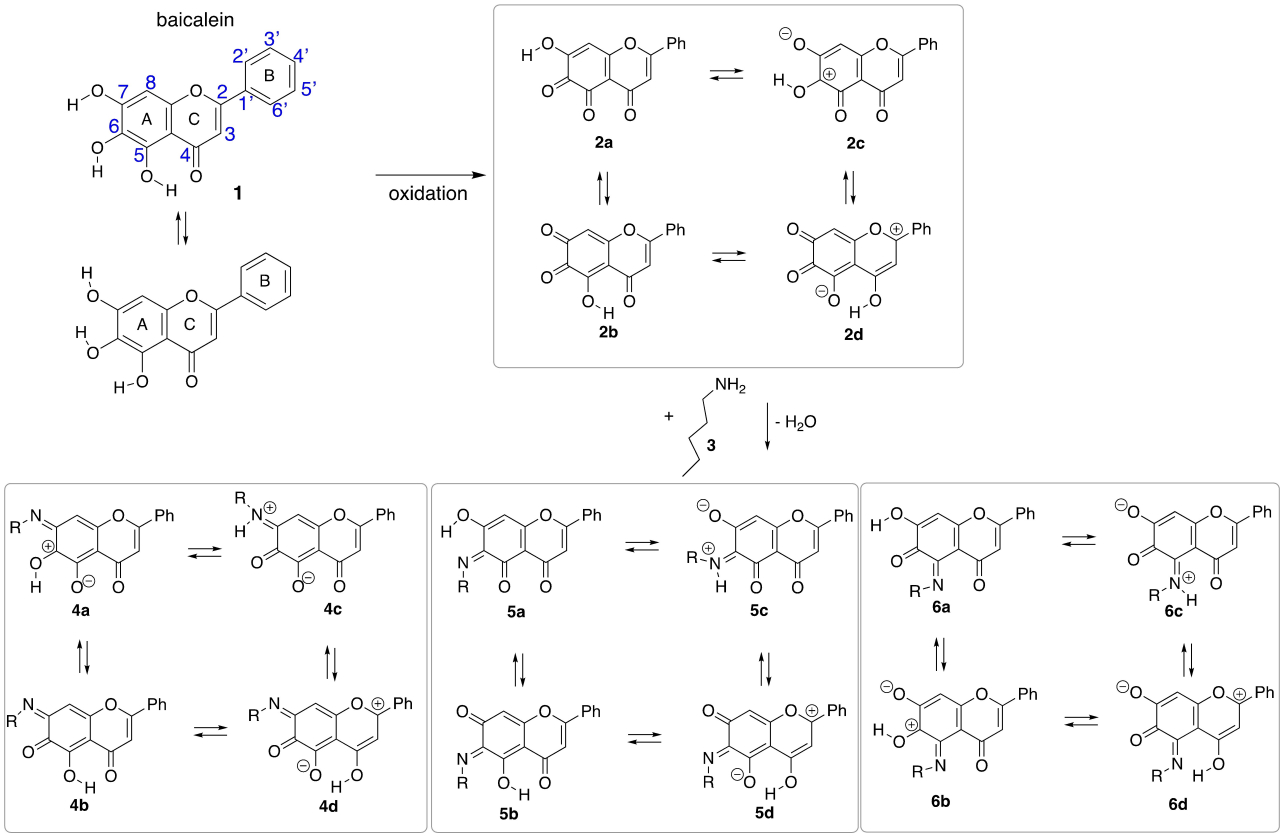

Scheme 2. Pathway from baicalein to dehydrobaicalein tautomers **2a**–**2d**, which will react with pentylamine to produce the covalently bound products **4a**–**4d**, **5a**–**5d** and **6a**–**6d**).

carbonyl group of C6 (2.25 Å), whilst in **2d** the proton of O4 orients to the neighboring C5–O, establishing a short interaction (1.77 Å) that anticipates an easy interconversion between **2d** and **2b** tautomers. Indeed, a relationship between the groups of C4 and C5 is also evidenced in studies in which the **BA** acts as a chelator and coordinates the metal by these adjacent groups.[35] The conformational reaction of the tautomeric shift between **2d** and **2b**, in the presence of one explicit water molecule, has activation and reaction energies of 15.0 and 10.2 kJ mol^{-1}, respectively (Figure S4). This quite small barrier suggests that the tautomeric exchange between **2d** and **2b** follows the Curtin-Hammett principle, in which two tautomeric species are conformationally equilibrated when their interconversion is much faster than the reaction that they can be involved.

Theoretical dehydrobaicalein–pentylamine (DBA–PA) tautomeric analysis

Because the nucleophilic attack of the amine group can occur at positions C7, C6 and C5 of the A ring, there are 12 different possibilities for formation of dehydrobaicalein–pentylamine adducts (**4a**–**4d**, **5a**–**5d** and **6a**–**6d** products of the reaction, Scheme 2). According to the relative energy values to the most stable tautomer (Table S3), the adduct formation at C7 (**4c**) is clearly favored, followed by C6 (**5a**, +23.5 kJ mol^{-1}) and C5 (**6c**, +24.7 kJ mol^{-1}) positions. It is interesting to note that two of these forms are zwitterionic in nature, where the iminium ion unit is actively involved in hydrogen bonding interactions with its direct neighbors. This energetic ordering is strongly impacted by aqueous solvation effects, and the predicted relative ordering in the gas phase can be thus substantially different.

Theoretical pK_a values of baicalein

Previous data obtained for fisetin (Scheme 1a) suggested a pH dependence for the regioselectivity and nature of the formed quinone adducts. At pH values bellow the pK_a for quinone protonation, they also observed the formation of water adducts in the C ring of the flavonoid (inexistent at pH > pK_a).[5] Considering the structural similarities of fisetin and baicalein, the pK_a values of the latter were determined to assess possible effects of pH on the quinone chemistry and the regioselectivity of the formed adducts by this electrophilic molecule. A computational approach to calculate relative pK_a values using a reference molecule was carried out. The reference flavonoids with known experimental pK_a values used in this study are: chrysin (which belongs to the flavone class as does **BA**, but has only two ionizable groups), and galangin (with three ionizable groups as in **BA**, but belongs to the class of flavonols). To validate the employment of the proton exchange method to determine the pK_a values of flavonoids, we first calculate the pK_a value of the 7-hydroxyflavone using chrysin and galangin as reference compounds (Schemes 1a, S2 and S3). As example of the procedure, Scheme 3 illustrates the thermocycle for the deprotonation reaction of 7-hydroxyflavone using chrysin as reference molecule.

The experimental pK_a values determined for 7-hydroxyflavone vary between 7.39 and 8.48,[36] which compares to the calculated pK_a values of 8.2 and 8.4 with the chrysin and galangin reference systems (Table 1). The same protocol based on the experimental pK_a values of chrysin (pK_{a1} = 8.0 and pK_{a2} = 11.9) and galangin (pK_{a1} = 7.6, pK_{a2} = 9.5 and pK_{a3} = 10.9) obtained by Musialik et al.[36] is then used for the calculation of the pK_a values of **BA**.

The electronic energies of the optimized geometries of all possible mono-, di-, and tri-anion species of the three flavonoids are in Table S1. For **BA**, our calculations indicate the deprotonation of the C7–OH group as the most favorable, which agrees with earlier studies pointing to this group as the most acidic (pK_a between 7.5 and 8.5) and the most favored for heterolytic O–H breaking.[33b,36] In addition, the di-anionic

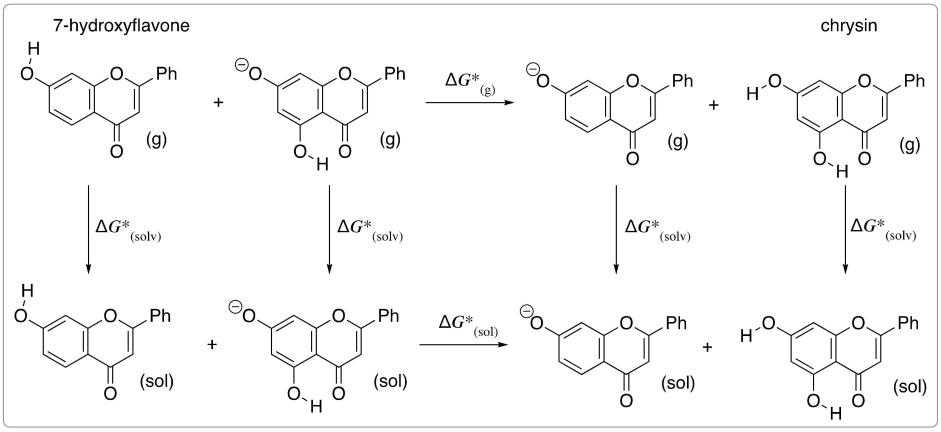

Scheme 3. Thermodynamic cycle for the deprotonation of 7-hydroxyflavone with chrysin as reference molecule.

Table 1. Computed pK_a values of the ionizable groups of 7-hydroxyflavone and baicalein with chrysin and galangin as reference molecules.

Reference	Target	SMD(water)/ B3LYP-D3/6-31 + G(d,p)	DLPNO-CCSD(T)/ cc-pVTZ//SMD(water)/ B3LYP-D3/6-31 + G(d,p)
chrysin (pK_{a1} = 8.0; pK_{a2} = 11.9)[36]	pK_{a1} (7-hydroxyflavone at C7–OH)	8.2	8.2
	pK_{a1} (**BA** at C7–OH)	6.2	5.5
	pK_{a2} (**BA**–7O$^-$ at C5–OH)	11.8	12.1
	pK_{a3} (**BA**–7O$^-$,5O$^-$ at C6–OH)	17.3	28.2
galangin (pK_{a1} = 7.6; pK_{a2} = 9.5; pK_{a3} = 10.9)[36]	pK_{a1} (7-hydroxyflavone at C7–OH)	7.9	8.4
	pK_{a1} (**BA** at C7–OH)	6.0	5.6
	pK_{a2} (**BA**–7O$^-$ at C5–OH)	14.4	15.4
	pK_{a3} (**BA**–7O$^-$,5O$^-$ at C6–OH)	15.1	24.5

molecule with positions 7 and 5 deprotonated is marginally more stable than the dianion-7,6-baicalein molecule (difference of 23.8 kJ mol^{-1}), thus suggesting an acidity order of C7 > C5 > C6. Table 1 displays the pK_a values for **BA** (following Schemes S2 and S3). The computed pK_{a1} of **BA** is 5.5 or 5.6, which is slightly smaller than the usually estimated for flavonoids, indicating that a significant portion of baicalein would be dissociated at pH 7.4 as well as in the alkaline conditions required to act as antioxidant. Our predicted pK_{a2} of **BA** is 12.1 or 15.4, which are 0.2 and 5.9 pK_a units larger than the experimental value of the reference molecules (chrysin and galangin, respectively). The pK_{a2} of 12.1 should be more reliable because the deprotonated position in **BA** is the same as those in the reference chrysin molecule. However, the use of both reference molecules estimates a somewhat large pK_{a3} value for **BA**, being 16.3 and 13.6 p*K*a units larger than the respective reference values. This discrepancy probably happens due to the distinct number of ionization groups in chrysin, as well as the different hydroxylation pattern in galangin: **BA** only has OH groups on its A ring, whilst galangin has the C3–OH group on the B ring that also establishes a hydrogen-bond with the carbonyl group at C4, decreasing the acidity of the C5–OH group. In addition, this structural difference can also influence the accuracy of the proton exchange method by introducing possible errors.[32] Furthermore, there are possible limitations of the implicit solvation model used in the calculations that may provide a poor description of multi-anionic species. Indeed, past theoretical studies on successive deprotonation reactions in aqueous solution (using the same solvation model) of flavonols indicated much larger Gibbs free energy differences after the second deprotonation.[37] Despite the error of the method, our results suggest large values for the second and third ionization, which can in turn influence the oxidation ability of baicalein to form quinone forms in alkaline environments.

Experimental studies of baicalein and its reaction with pentylamine

Selected NMR and HRMS experiments were performed to characterize baicalein and its reactivity with pentylamine in solution, which is not known. The ^{1}H NMR spectrum of partially deuterated [D$_2$]**BA** reveals the loss of 6-OH and 7-OH peaks, although a weak 5-OH signal remains detectable for slightly longer times, indicating a constrained proton position (Figure S5). This is in full agreement with earlier experiments, in which the alkylation of **BA** with *n*-propyl iodide in acetone generated a mixture of two products: one monoalkylated at position C6 (11%) and another molecule dialkylated at positions C6 and C7 (62%; Scheme S4).[38] It was proposed that the 5-OH of **BA** forms an intramolecular H-bond with the keto group, which reduces its reactivity. Previous theoretical studies also pointed out the most stable radical tautomer was obtained by dehydrogenation of the C6–OH group of **BA**, whilst the most stable anion tautomer of **BA** was obtained by deprotonating the C7–OH.[33b]

In order to explore the intrinsic reactivity of baicalein's A ring substructure, initial experiments with **PA** involve 2′,3′,4′-trihydroxyacetophenone (**7**, **TAP**) as a simplified model. Mixing **TAP** with **PA** in CH_2Cl_2 leads to the immediate formation of a yellow crystalline precipitate, whose characterization by NMR spectroscopy indicates a 1:1 ratio of the constituting reactants **TAP** and **PA**, but no signal correlations (and thus no covalent bonding) between the respective fragments. This is most easily understood through formation of the **TAP**-**PA** ammonium-phenolate ion pair shown in Scheme 4, whose assignment is also supported by the solid state structure of the precipitate (Figure S7 and Table S4, CCDC deposition number 2124561). This agrees with the well-known tendency of phenols to form rather stable hydrogen-bonded complexes with amines.[39] On extended reaction times the **TAP**–**PA** complex was then observed to form imine **8** at room temperature (Scheme 4).

Due to its structural resemblance with **TAP**, we expect an analogous behavior for baicalein (**1**, **BA**) in its reaction with pentylamine. Due to the very low solubility of **BA** in CH_2Cl_2 these reactions have been performed in [D$_6$]DMSO under nitrogen atmosphere (see the Supporting Information for details). As anticipated, the ^{1}H,^{13}C HSQC spectra shows the formation of **BA**–**PA** salt species; however, no formation of the imine condensation product could be observed even after 72 h at room temperature or after 5 h at 50 °C (Scheme 5). The proposed deprotonated **BA**$^-$ structure is based on the similar chemical shifts of **TAP** data, and indeed it is in line with the first deprotonation position (pK_{a1}) of **BA** predicted by QM calculations. The obtained **BA**–**PA** salt structure is also in line with the formation of ion pairs in the reaction of hexamethylenediamine with catechin (as model for tannin extracts).[40]

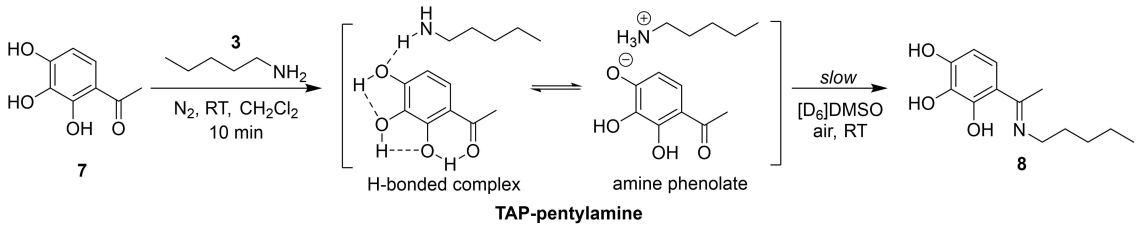

Scheme 4. Reaction of **TAP** with **PA**.

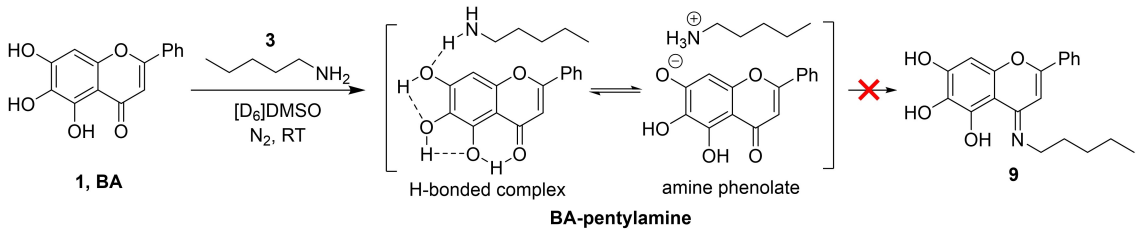

Scheme 5. Reaction of **BA** with pentylamine under anaerobic conditions.

Therefore, these results suggest an effective role of oxygen as initiator of the reaction between the **BA** and **PA**. In fact, a past study also showed that the flavonoid epigallocatechin (EGC, Scheme 1) treated with aqueous ammonia solution under aerobic conditions forms a condensation adduct.[15a] A similar behavior was also reported by Velander et al.[4b] after incubating **BA** for 4 days with the hIAPP amyloid polypeptide in Dulbecco's phosphate buffer solution containing 2.25% DMSO (*v*/*v*). Even though the oxidized product species was not directly detected in these studies, they characterized the final product by LC–MS as reduced baicalein–hIAPP conjugate (Scheme 1b). They proposed that **BA** can be autoxidized to *o*-quinone that conjugates with hIAPP amine groups through a Schiff base mechanism with further reduction.[4b]

To evaluate the impact of aerobic conditions in this reaction, the nitrogen atmosphere was replaced by pure oxygen, whereupon the solution promptly changes from orange to black, and then to deep red. Even the exposure to air during sample preparation for NMR analysis can trigger the reaction, supporting the role of oxygen/air to initiate the reaction. Also, it has been shown that when freeze-pump-thaw degassed solvents are used no condensation product is detected (see the Supporting Information for details). The APCI-MS analysis shows a $[M+H]^+$ peak at *m/z* 340 corresponding to an amine condensation product, and the $^1H,^{13}C$ HMBC NMR analysis reveals that the regioselectivity is at C6 (C6-substituted **BA** derivative). The molecular geometry and energy of all tautomers and rotamers of the various **BA**–**PA** product ($[M+H]^+$ peak at *m/z* 340) were analyzed with the same theoretical methods as before. **BA**–**PA 10a** (C7-substituted) and **11a** (C6-substituted) are found to be the most stable in an aqueous environment, and their very small energy difference (3.3 kJ mol^{-1}) suggests that both tautomers are populated at ambient temperature, which agrees with the observed experimentally.

Experiments on BA oxidation and dehydrobaicalein–pentylamine condensation reaction

Some studies indicated that baicalein (**BA**) exhibited antioxidant and free radical-scavenging activities (scavenged hydroxyl radical, 2,2-diphenyl-1-picrylhydrazyl (DPPH) radical and alkyl radicals in a dose-dependent manner in alkaline solution).[41] The formation of **DBA** was also detected by previous UPLC/ESI-MS studies with baicalin, a glucuronide form of **BA** (Scheme 1a).[42] However, previous experimental attempts of structural investigation of **DBA** in solution are not so widely known. Because of this, we assess the reactivity of baicalein with molecular oxygen through in situ oxidation of **BA** by a flow of pure O_2 for 15 h in $[D_6]$DMSO. However, no major differences could be observed in the analytical data after this treatment, which indicates that **BA** is stable under these conditions. This lack of reactivity is supported by a theoretically calculated reaction free energy of $+22.7$ kJ mol^{-1} for the reaction of triplet oxygen with **BA** to yield hydrogen peroxide and **DBA**. Afterwards, several experiments with increasing pH values were carried out (details in the Supporting Information). The obtained results are in line with earlier studies of Feng et al.,[43] where it was shown that even under mild conditions **BA** tends to degrade at higher pH values. All this data reinforces the idea that the formation of **BA**–**PA** ion-pair species (H-bonded complex or ammonium phenolate) is a crucial step, since the deprotonated **BA**$^-$ readily oxidizes and forms **DBA** as a transient intermediate. In order to assess the condensation reaction of the *o*-quinone dehydrobaicalein with **PA** in solution, a protocol with *o*-chloranil as an alternative oxidant to oxidize **BA** is used.[44] APCI-MS analysis shows successful formation of **DBA** through its $[M+H]^+$ ion peak at *m/z* 269, whilst the $^1H,^{13}C$ HMBC NMR analysis characterizes the structure of **DBA** as 6,7-dehydrobaicalein. Further, the formation of **DBA** was also examined by treating the obtained crude **DBA** with an excess

of *o*-phenylenediamine in MeOH with a catalytic amount of acetic acid in analogy to an established procedure by Morimoto and colleagues.[45] The analytical data gathered by APCI-MS ($[M+H]^+$ signal at *m/z* 341) for the crude reaction products are in line with the already characterized 6,7-substituted **BA** phenazine derivative,[45] which also supports the formation of **DBA 2b** species throughout the reactions.

Afterwards, the obtained crude **DBA** was treated with **PA** in CH_2Cl_2 and with a catalytic amount of glacial acetic acid.[44] The APCI-MS analysis indicates coupling products distributed in two $[M+H]^+$ ion peaks (at *m/z* 336 and *m/z* 340) with a ratio of ~3/2, as well as a peak of reduced baicalein species (*m/z* 271). However, these mass spectrometric peaks have a difference of about *m/z* 2 to the expected $[M+H]^+$ ion peak at *m/z* 338 for the imine adduct (**4a**–**4d**, **5a**–**5d** or **6a**–**6d** in Scheme 2). Overall, this data is consistent with a Schiff base reaction, in agreement with the baicalein–hIAPP covalent Schiff base conjugation proposed by Velander et al.,[4b] and discards the mechanistic hypothesis of the aza-Michael addition characterized for some *o*-quinone species of flavonoids.[6c] Also, the molecular geometry and energies of the possible tautomers and rotamers of product with the $[M+H]^+$ peak at *m/z* 336 were analyzed with the same theoretical methods as before. Based on the results of this study, we propose the mechanism of the Schiff base reaction between **BA** and **PA** shown in Scheme 6. The reaction energies of the main mechanistic pathways, predicted by QM calculations using the experimentally observed tautomers, are displayed in Scheme S17.

According to Scheme 6, **BA** reacts anaerobically with **PA** to an ion pair intermediate with 1:1 composition. This ionic structure is very susceptible to oxidation by O_2 and thus reacts rapidly to **2b**, which subsequently forms the Schiff base condensation product (**5a**, $[M+H]^+$ at *m/z* 338) at the most electrophilic carbonyl (C6). However, this transient intermediate product is straightaway reduced by another **BA** molecule to afford the product **11a** with $[M+H]^+$ at *m/z* 340 and regenerates **DBA**. As the latter reaction is found to be endergonic at $+18.9\ kJ\,mol^{-1}$, the driving force to obtain the main product observed experimentally (**11a**) is the formation of the transient intermediate **5a** (which is found to be largely exergonic, $\Delta G_R = -61.2\ kJ\,mol^{-1}$). Similar redox cycles have also been proposed for alike oxidative reactions,[15b,16d] such as those between catechin derivatives and nucleophiles.[15a] An important characteristic of this *ortho*-quinone chain mechanism is the requirement of only minute amounts of oxygen for the generation of the amine coupling product **11a**, which may also provide a rational basis for the observation of residual inhibitory activity of baicalein under formally anaerobic conditions.[6b]

Furthermore, to uncover the further formation of product **14a** with $[M+H]^+$ at *m/z* 336, some control experiments (detailed description is provided in the Supporting Information) were carried out. On the one hand, the oxidation of the C6-substituted **BA** derivative **11a** ($[M+H]^+$ at *m/z* 340) leads to the formation of the highly oxidized adduct **14a**, while at the same time reducing **DBA** back to **BA**. Two molecules of **DBA** are needed for this coupling reaction that is found to be exergonic at $-106.7\ kJ\,mol^{-1}$. On the other hand, not detecting of product **14a** ($[M+H]^+$ at *m/z* 336) in the experiments under a mild oxidant agent (e.g., air) suggests that this extra reactive pathway only occurs in the presence of strong oxidants such as *o*-quinones. All proposed reaction pathways are viable in a cell environment due to several oxidant and reactive species produced by enzymatic or nonenzymatic reactions that could assist in **DBA** formation. That at least two molecules of **DBA** are needed for the coupling reaction to yield **14a** ($[M+H]^+$ at *m/z* 336) suggests that the **DBA** amounts in solution (or in human physiological conditions) act as a regulator to thereby direct the redox chain reaction to form the product **11a** or **14a**.

Another rational mechanistic hypothesis would be the disproportionation of two molecules of **5a** to form products **11a** and **14a**. This reaction is found to be exergonic at $-69.0\ kJ\,mol^{-1}$, which provides an additional argument for why direct detection of Schiff base product **5a** was not successful. All taken together the experiments clearly show the oxidation of baicalein in solution as well as the formation of the reduced and highly oxidized covalent dehydrobaicalein-amine adducts. The latter observations are particularly relevant to complement the computational study on the reaction mechanism for **DBA**–**PA** Schiff base formation.

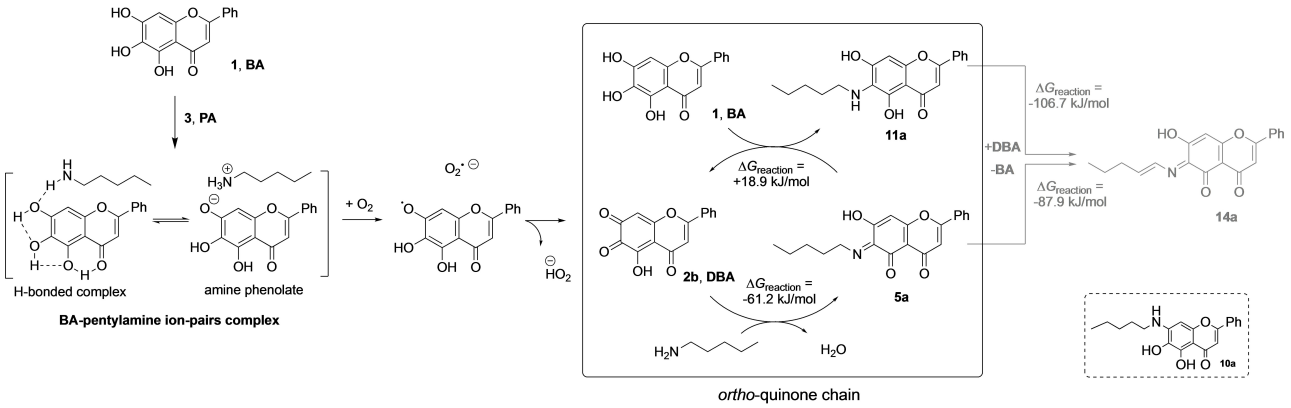

Scheme 6. Proposed mechanism for the condensation reaction between **BA** and **PA**.

BA is known to be a strong iron chelator under physiological conditions, in which the O6 and O7 atoms constitute the iron-binding site.[46] In general, in the presence of redox-active ions, the flavonoids might act as antioxidants or as pro-oxidants, affecting the metal-promoted Fenton chemistry and the redox state of cells. On the other hand, in the presence of amyloid peptides, the metal ions can interact with them and create hydroxyl radicals, which could accelerate the production of flavonoid–quinone species. Hence, the presence of transition metals could help the redox shuttling required for the **BA**–**PA** condensation reaction in an unspecific manner. Regarding the anti-amyloidogenic properties of the flavonoids in the presence of metals, it was observed that the Zn–EGCG complex significantly suppress hIAPP's amyloid aggregation and cellular toxicity,[47] whilst the Al^{III}–EGCG complex inhibits hIAPP fibril formation more efficiently than the flavonoid alone.[48] However, the underlying molecular details of these reactions are not yet fully understood. Grasso et al. also indicated that in an oxidative stress-related environment, Cu^{II} ions generally inhibit the Michael addition modification between the 4-hydroxy-2-nonenal and the His residues of Aβ. However, once it is formed, the metal still binds the peptide with high affinity, forming a ternary complex.[49] Despite possible competition effects, these studies suggest that the **BA**–**PA** Schiff base reaction may progress in a medium with metal ions; however, all these processes merit further investigation.

Many studies reported that the covalent modifications of proteins by quinones may severely influence the properties of both reaction partners, which is particularly important when amyloid proteins are involved. In general, protein–flavonoid covalent complexes have higher stability and protect the phenolic compound from decomposition. The main molecular events of amyloid formation are the primary and secondary nucleation, fibril elongation and fibril fragmentation.[2a] Zhu et al. showed that the **BA**-α-synuclein adducts affect the nucleation stage of aggregation by stabilizing stable and soluble oligomeric forms (off-pathway oligomers). The covalent binding of the **DBA** changed the secondary structure of the peptide, modifying the structural flexibility associated to the fibrils folding. Additionally, the covalently modified peptides were able to form oligomers with unmodified molecules.[6b] The same authors also observed the formation of stable hydrophilic oligomers by covalent binding of the oxidized quercetin to α-synuclein, leading to the inhibition of fibrillization by preventing both nucleation and elongation molecular events.[6a] Sato et al. suggested that the nucleophilic addition to the *o*-quinone form of the flavonoid (+)-taxifolin by the Lys residues of Aβ42 interferes more in the elongation rather than the nucleation phase.[8] As the structural flexibility and solvent exposure of lysine residues can facilitate their transitory deprotonation and favors the inhibition of amyloid aggregation by covalent binding,[6c] an effective inhibition of hIAPP aggregation by **DBA** is expected because the Lys1 belongs to the flexible N-terminus.

Theoretical DBA–PA Schiff base reaction mechanisms

To assess the regioselectivity of the **DBA**–**PA** Schiff base reaction mechanisms, we provide a detailed atomistic description of the overall mechanistic pathways and energetic portrait to attain the **4c**, **5a** and **6c DBA**–**PA** adducts. Throughout this discussion, all energies are those obtained at the DLPNO-CCSD(T)/cc-pVTZ//SMD(water)/B3LYP-D3/6-31 + G(d,p)) level of theory.

Formation of the 4c adduct

Considering that both **2d** and **2b** tautomeric forms (in conformational equilibrium) are those that provide possibilities for adduct formation at C7, we start our calculations by determining the tautomerization of the C4–OH group to a C4–keto group in the presence of pentylamine and one water molecule. The inclusion of an explicit solvent molecule assists the proton transfer leading to the final products, as has been described in previous studies.[16c,17] Figure S21 illustrates the stationary points for this reactive step as well as their associated energies. The activation and reaction energy are similar to those obtained in the absence of the amine group (differences of −3.2 and −1.5 kJ mol^{-1}, respectively), reinforcing the ease of the tautomeric conversion between **2d** and **2b**, with the latter showing itself as the most favorable to continue the reaction. The reaction then follows the well-established mechanism for Schiff base formation through nucleophilic attack of pentylamine at the C7–keto group, accompanied by water-mediated proton transfer from the amine to the carbonyl oxygen. Figure 1a shows the geometries of the stationary points of this step. In the reactant complex (react), the N atom of pentylamine is placed at distances of 2.77 and 2.31 Å from the C7 and C6 atoms of the A ring, respectively. The preference of the amine group to be positioned below the C6 atom seems to occur due to a charge distribution effect. Indeed, the natural bond orbital (NBO) analysis of tautomer **2b** (Figure S22) indicates that the charges of C6 and O6 (+0.498 and −0.508) are slightly higher than at C7 and O7 (+0.446 and −0.619), becoming more attractive for the nitrogen atom. The initially formed zwitterionic intermediate (react') then features an N–C7 distance of 1.57 Å and a largely pyramidalized carbonyl carbon atom. Hydrogen-bonded pre-reaction species were also observed in other studies on the reaction of amines and aldehydes.[16a,c] In the current case the energy difference between react' and react amounts to +46.9 kJ mol^{-1}. The following transition state TS1 is destabilized by additional 28.5 kJ mol^{-1} relative to adduct react' and characterized by an N–C7 distance of 1.52 Å and a short hydrogen bond of 1.47 Å between one of the amine protons and the water oxygen atom such that an energetically favorable six-membered ring arrangement is formed (Figure 1a). Starting from the resulting carbinolamine intermediate INT1 located +19.8 kJ mol^{-1} higher than the reactant complex react, various alternative pathways for its dehydration to the corresponding Schiff base were assessed.

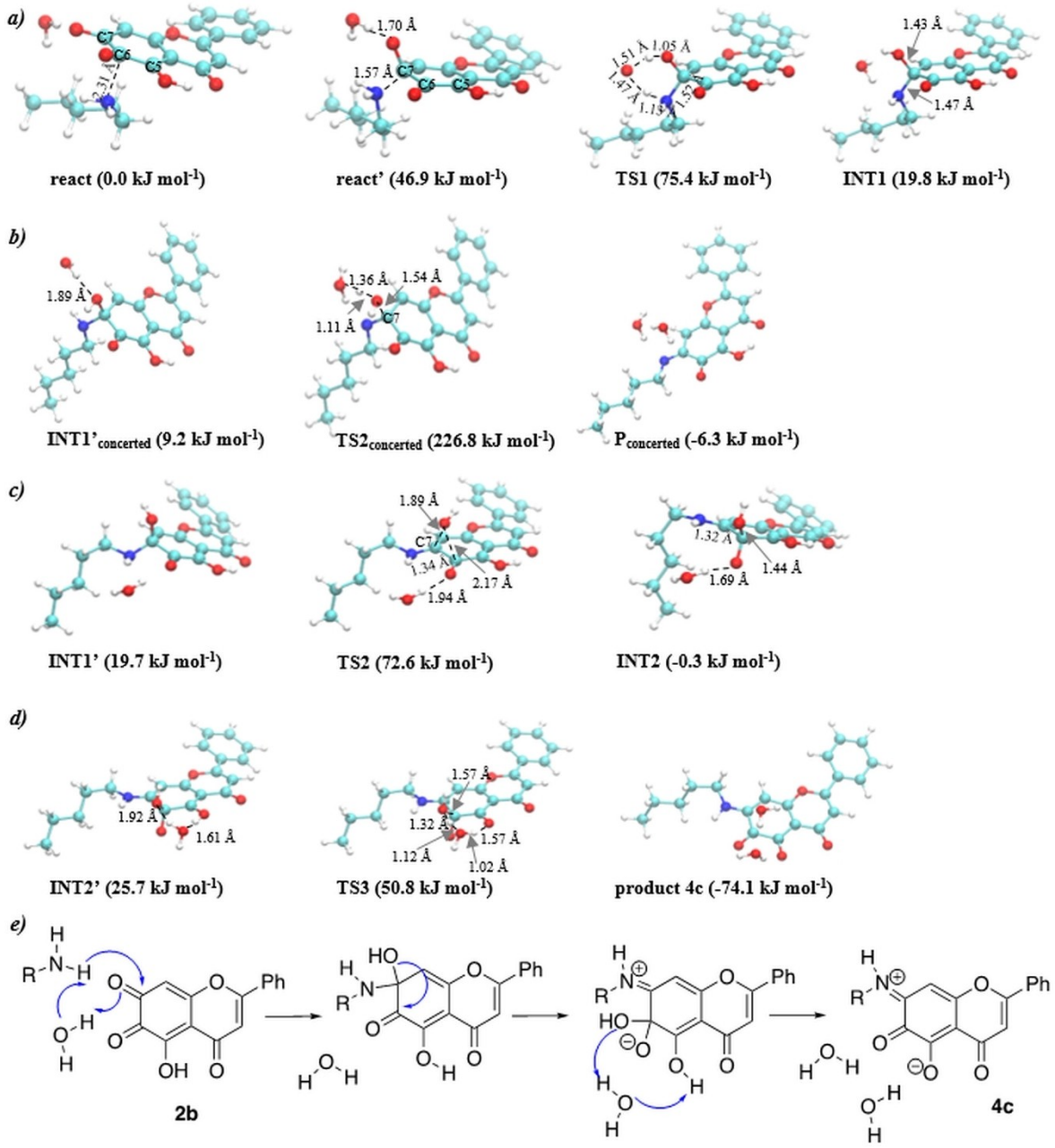

Figure 1. Representation of the mechanistic pathway to form the dehydrobaicalein–pentylamine adduct **4c**: a) carbinolamine formation, b), c) and d) dehydration/Schiff base formation, and e) 2D depiction of the complete reaction.

Firstly, the concerted release of the hydroxy group from C7 with the water-mediated transfer of one proton from the charged nitrogen, forming the neutral form of Schiff base (Figure 1b), is determined. The transition state $TS2_{concerted}$ features a six-membered ring geometry and faces a barrier of 217.6 kJ mol^{-1} relative to intermediate $INT1'_{concerted}$. In addition, the complete reaction is slightly exergonic ($\Delta G_R = -6.3$ kJ mol^{-1} relatively to react). Past studies pointed out the carbinolamine dehydration as the rate-limiting step, being in general, difficult and associated with large barriers (the inclusion of two water molecules still produces barriers of ca. 108 kJ mol^{-1}).[17] However, these activation energies could be dropped by assistance of other molecules such as polar groups or large solvent chains that allow efficient charge delocalization by hydrogen-bond networks. For example, the presence and involvement of functional groups such as the pyridoxal 5′-phosphate (PLP), a key co-enzyme in the metabolism of amino acids and inhibition of glycation in membrane surfaces, is critical to reduce the energy barriers and lead to faster imine formation.[16b,50] Therefore, our extremely high barrier means that this mechanistic path should be different than the usually postulated, or that additional solvent molecules are needed.

An alternative pathway for the dehydration reaction could be found, where the hydroxy group initially migrates from C7 to the neighboring C6 atom. The geometries of all stationary points are displayed in Figure 1c. INT1 and INT1′ are conformational isomers of each other with different positions for the assisting water molecule. Similar variations associated with small energy differences were also reported in earlier studies such as the nitrogen inversion.[17] Between INT1′ and the transition state TS2 the C7–OH bond distance increases from 1.46 to 1.89 Å, being severely weakened, but not yet broken. At TS2, the hydroxy group is positioned 2.17 Å away from C6, being bound only at the final state of this step (INT2). Throughout this step, the water molecule plays a stabilizing role on the carbonyl group of C6, and we can also see the expected hybridization change from sp^3 to sp^2 of the C7 atom. This step features a barrier of 52.9 kJ mol^{-1} and a reaction free energy of 20.0 kJ mol^{-1} relative to INT1. Then, in the last mechanistic step, the C5–OH transfers the proton to the assisting water molecule, which in turn donates its proton to the leaving hydroxy group (now bound at the nearby C6), yielding the protonated Schiff base and a second water molecule. As seen in Figure 1c, in the transition state TS3 the O5 is already deprotonated (O5–H distance of 1.57 Å), whilst the proton from the water is midway to the releasing hydroxy group (O_{wat}–H_{wat} and H_{wat}–OH distances of 1.12 Å and 1.32 Å, respectively), having the latter a HO–C6 distance of 1.57 Å. The TS3 is destabilized by 25.1 and 50.8 kJ mol^{-1} relative to the INT2′ and react states, respectively. Additionally, the product state is energetically favored relative to INT2′ by −99.8 kcal mol^{-1}, which brings the overall reaction free energy to −74.1 kJ mol^{-1}.

As can be seen in the mechanistic summary in Figure 1e, the overall dehydration/Schiff base formation sequence occurs in two separated steps, which differs from that commonly expected for this reaction (concerted release of the hydroxy group with N=C formation). This difference can derive from the particular structure of the A–C rings (resonance effects) and could be a specific property of the dehydrobaicalein species.

To investigate the effect of more solvent molecules, additional calculations were performed on this reaction mechanism considering a second explicit water molecule (see the Supporting Information for details). The results support a similar reaction pathway as compared to that established for only one water molecule. However, the inclusion of an additional water molecule greatly facilitates all mechanistic steps by assisting the proton transfers or through a neighboring catalyst charge delocalization effect. As a consequence, the barriers of the carbinolamine and dehydration steps decreased by 16.2 and 12.7 kJ mol^{-1}. This is in agreement with previous calculations on imine formation from methylamine and formaldehyde, where the inclusion of two water molecules greatly reduced the barrier for carbinolamine formation.[17] Several reaction coordinates were tested to establish the reported dehydration step through the energetically favored eight-membered ring transition states. However, all these attempts were unfruitful probably due to stereoelectronic effects of the bulky and strained A–C rings of dehydrobaicalein.

Formation of 5a adduct

Two reaction pathways were explored for the formation of **5a**, one starting from tautomer **2a** and the other starting from tautomer **2b**. Figure 2 illustrates the geometries of key stationary points along the pathway that is similar to that described for **4c** before.

Starting from **2a**, the reactants feature a N–C6 distance of 2.20 Å that shortens to 1.54 Å in transition state TS1. This latter state resembles a six-membered ring with an internal CNH angle of 99.7°, the O6 is almost protonated (H_{wat}–O6 distance of 1.08 Å) and the amine is transferring its proton to the assisting water molecule (N–H and H–O_{wat} lengths of 1.14 Å and 1.45 Å). TS1 lies 43.7 kJ mol^{-1} above the reactant complex, while the following carbinolamine intermediate INT1 lies 16.9 kJ mol^{-1} below the reactants. The dehydration/imine formation step is, however, rather different to the one found previously for adducts **4c** and **6c**. It becomes simpler due to the neighboring C7–OH unit that can donate its proton to the leaving C6 hydroxy group that releases a water molecule and forms the protonated Schiff base. The assisting water plays a catalytic role by electrostatic stabilization of O7 the oxygen atom. The following transition state TS2 features C–O and N–C bond distances of 1.55 and 1.39 Å, whilst the H-transfer is already advanced, being the proton nearer to the hydroxy group (distance of 1.12 Å) than to the O7 (distance of 1.37 Å). The barrier for this step amounts to +69.1 kJ mol^{-1} relative to INT1′, whereas the formed intermediate **5c** is favored by 27.1 kJ mol^{-1} relative to the reactant complex. The sequence terminates through H-transfer to form product **5a**. In the associated TS3, the proton from the nitrogen is already transferred to the water molecule (distances of 1.41 Å and 1.11 Å, respectively), whereas the other proton is being transferred to O7 (distance of 1.36 Å). The barrier for this step is +35.6 kJ mol^{-1} in relation to INT2′, and the complete reaction is exergonic by ΔG_R = −32.5 kJ mol^{-1}.

As expected, a similar reaction pathway can be found when starting from **2b** (Scheme 7). The main difference between the two reactions is found in the energy profile, where the barriers for carbinolamine and Schiff base formation generated by the latter tautomer are higher by 16.3 and 12.7 kJ mol^{-1}, respectively.

Formation of 6c adduct

Scheme 8 portrays the reaction pathway for the formation of **DBA**–**PA** adduct **6c** from the **2a**. The complete reaction is exergonic at −49.0 kJ mol^{-1}. Despite the similarity of the reaction pathways leading to adducts **6c** and **4c**, there are some differences in the reaction energy profiles. The barrier for formation of the carbinolamine intermediate is much smaller in the formation of **6c** than the formation of **4c** with an energy differences of 48.5 kJ mol^{-1}; however, the latter adduct is thermodynamically more favorable by 16.2 kJ mol^{-1}.

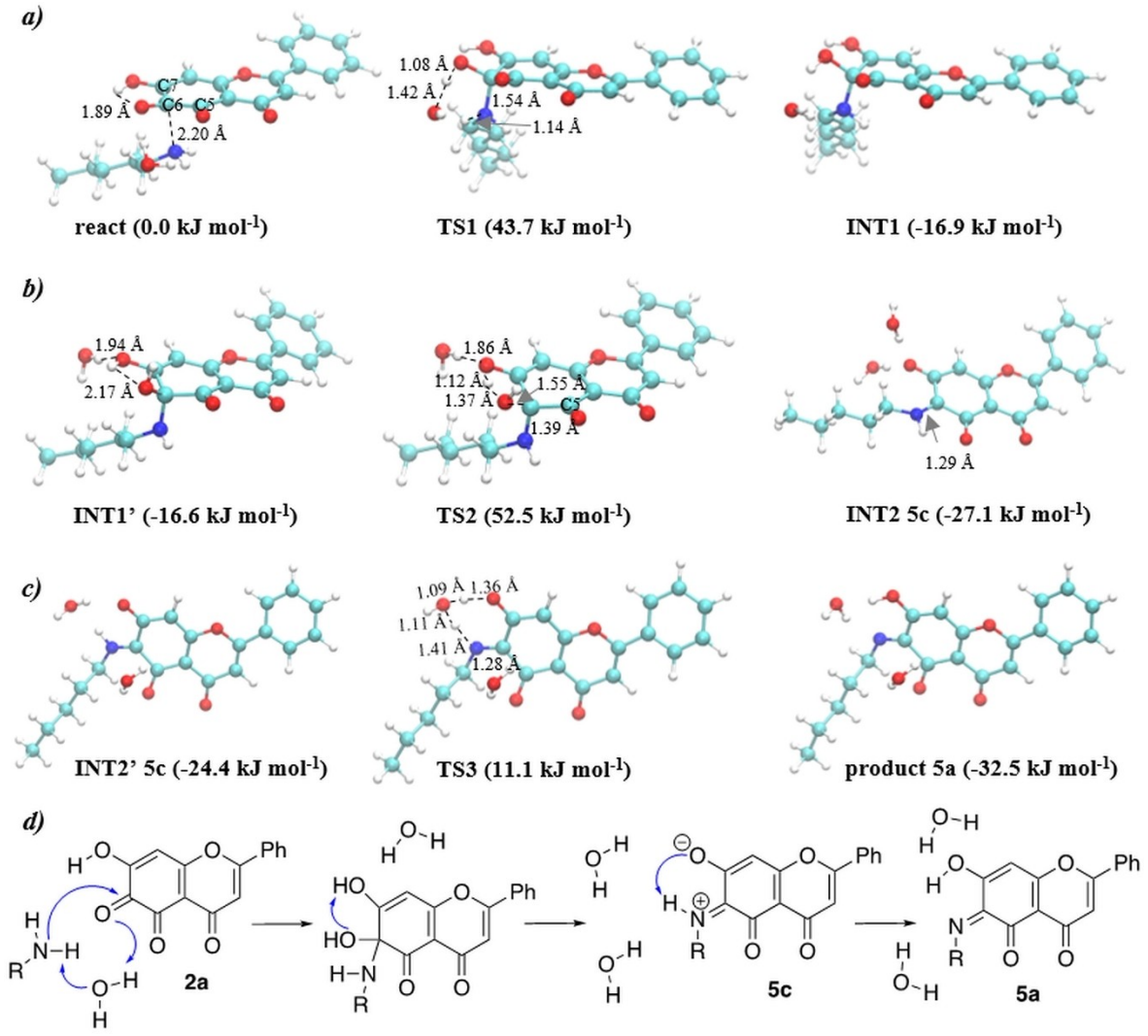

Figure 2. Representation of the mechanistic pathway to form the dehydrobaicalein–pentylamine adduct **5a** from **2a**: a) carbinolamine formation, b) dehydration/Schiff base formation, c) **5a** formation, and d) 2D depiction of the complete reaction.

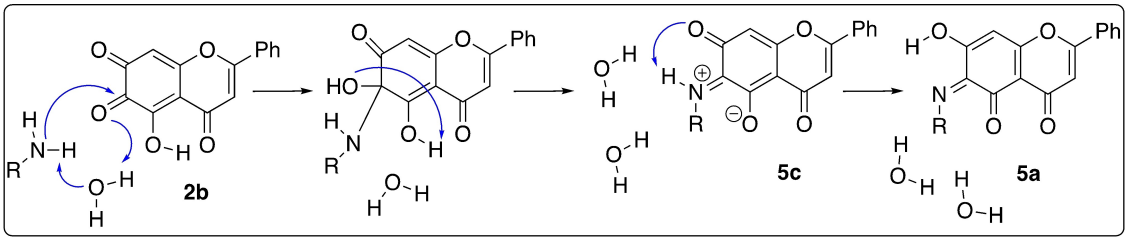

Scheme 7. Reaction pathway for the formation of dehydrobaicalein–pentylamine adduct **5a** from **2b**.

Energetic comparison of the reaction pathways to form the 4c, 5a and 6c adducts

Figure 3 displays the energy profiles for the complete reaction pathways to form adducts **4c**, **5a** and **6c** in the presence of one water molecule as obtained at the DLPNO-CCSD(T)/cc-pVTZ//SMD(water)/B3LYP-D3/6-31+G(d,p) level of theory. For the cases with two geometries of the same species (e.g., INT1 and INT1′), the most favored state is considered to compare the energies of the various mechanisms. These results show higher free energies for the dehydration step of all reactions (varying between 69.4 (**5a** path from **2a**) and 87.0 kJ mol^{-1} (**6c** path)), thus indicating that this step should be rate-limiting. The exception is the path to form **4c** that, due to a charge

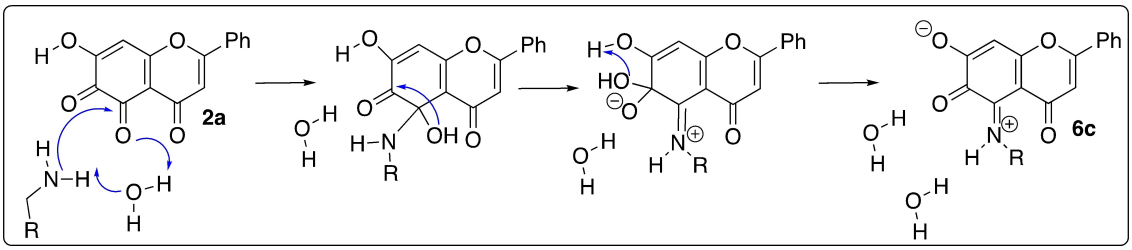

Scheme 8. Mechanistic pathway from **2a** to form the dehydrobaicalein–pentylamine adduct **6c**.

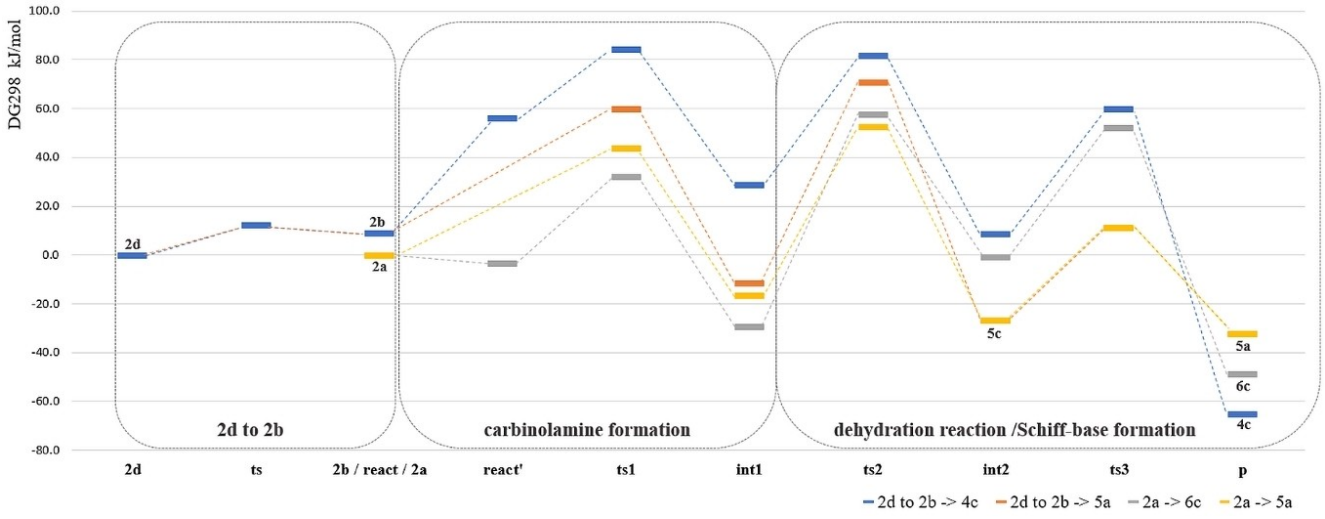

Figure 3. Energetic profiles of the Schiff base reaction of dehydrobaicalein tautomers **2a**, **2b** and **2d** with the nucleophile **3** to yield the dehydrobaicalein–pentylamine adducts **4c**, **5a** and **6c**.

delocalization effect on **2b** structure that provides a disadvantageous pre-reaction geometry, has similar barriers for carbinolamine and Schiff base formation (84.2 and 81.4 kJ mol^{-1}, respectively). This unfavorable effect is also reflected in the instability of the carbinolamine intermediate on the **4c**-path (28.6 kJ mol^{-1} above the reactants) that is notoriously different to the energetically favored intermediates of the other reactions (−29.6 kcal mol^{-1}, −16.9 and −11.5 kJ mol^{-1} for **6c** path, **5a** path (from **2a**) and **5a** path (from **2d**/**2b**), respectively).

Overall, these mechanistic findings indicate energetically viable routes to form the various **DBA**–**PA** adducts, which could be responsible for the favored covalent inhibition mechanisms of baicalein targeting lysine residues of amyloid proteins. The formation of **5a** (C6-substituted **DBA**) is kinetically favored due to the overall lowest free energy barriers, while the formation of **4c** (C7-substituted **DBA**) is found to be the most thermodynamically favored (exergonic at −65.2 kJ mol^{-1}). The experiments only found the C6-substituted Schiff base product, which suggests kinetic control under these reaction conditions.

Furthermore, considering the higher stability of **4c**, future **DBA**-based drug-design strategies should focus on providing molecules with further positive charge character nearby the C7 (e.g., at C8) centers to improve the relative amine group C7 position, avoiding the formation of the unfavorable pre-reaction geometry that subsequently may decrease the barriers.

Conclusions

Amongst its physiological antioxidant benefits, the flavonoid baicalein exhibits inhibitory activity towards amyloid proteins such as hIAPP through covalent reactions with the pentylamine group of lysine residues that subsequently disturb the peptide aggregation. A combination of in silico and in vitro approaches is essential to clarify the oxidation state and reactivity of **BA** as well as its conjugation with the side chain of lysine residues in solution.

Based on these results, we conclude that: i) dehydrobaicalein species, namely 6,7-dehydrobaicalein **2b**, are formed in solution. ii) The reaction of **BA** and **PA** starts with the formation of a ion pair between the protonated amine group and the ionized **BA**$^-$ under anaerobic conditions that precedes a (low-oxygen) induced redox chain reaction. Thus, the presence of O_2 is crucial to generate the *o*-quinone **DBA** that promptly forms the intermediate **DBA**–**PA** (**5a**), which could be then reduced to yield the main **BA**–**PA** product (**11a**). Despite the fact that transient intermediate **5a** could not be detected under our

experimental conditions, we propose that its formation and further reduction is essential for the redox cycle. iii) The atomistic mechanistic studies uncovered an unusual pathway for the carbinolamine dehydration reaction, which focuses on the resonance ring effects of the dehydrobaicalein species. It involves an intramolecular rearrangement of the hydroxy leaving group that assists and reduces the barrier of this step. Also, the carbinolamine dehydration mechanistic step of all studied pathways is the rate-limiting step. iv) In agreement with the kinetically preferred pathway suggested by calculations, experiments show a regioselectivity of the Schiff base reaction for the middle position of the three hydroxy groups of **BA**. This may be attributed to the resonance-stabilized structure along the AC and B (with no substituents) rings. However, the theoretical mechanistic findings suggest feasible energetic profiles for all reactive pathways toward the formation of C6-, C7- and C5-substituted products. These many covalent mechanistic possibilities could be a specific property of baicalein that might contribute to its higher inhibition ability against amyloid formation as compared to other structurally related flavone molecules. The poor solubility of baicalein could limit its use as a therapeutic compound, but innovative strategies such as the use of baicalein–theophylline cocrystals have been proposed to overcome this hurdle and improve the bioavailability of baicalein.[51] In addition, a baicalein-β-cyclodextrin combination was suggested as a promising therapeutic route to inhibit and remodel α-synuclein amyloids.[52] These should be considered in designing novel baicalein-based molecules for inhibiting hIAPP amyloidogenesis in vivo. The pharmacological and wide structural properties of flavonoids as well as their lower toxicity compared to synthetic compounds gives them an advantage as future multitargeting therapeutic molecules. Hence, the currently uncovered mechanistic differences could be valuable to optimize and engineer future *o*-quinone–baicalein based drug candidates.

Acknowledgements

This work was supported by UIDB/50006/2020 with funding from FCT/MCTES – the Portuguese Foundation for Science and Technology through national funds. N.F.B. acknowledges support from the scientific employment stimulus – individual call of 2018 (CEECIND/02017/2018). Open Access funding enabled and organized by Projekt DEAL.

Conflict of Interest

The authors declare no conflict of interest.

Data Availability Statement

The data that support the findings of this study are available in the supplementary material of this article.

Keywords: autoxidation · computational chemistry · quinones · Schiff bases · transition states

[1] X. X. Zhang, Y. H. Pan, Y. M. Huang, H. L. Zhao, *World J. Diabetes* **2016**, *7*, 189–197.
[2] a) V. Armiento, A. Spanopoulou, A. Kapurniotu, *Angew. Chem. Int. Ed.* **2020**, *59*, 3372–3384; *Angew. Chem.* **2020**, *132*, 3396–3409; b) M. Stefani, S. Rigacci, *Int. J. Mol. Sci.* **2013**, *14*, 12411–12457.
[3] a) Z. Dhouafli, K. Cuanalo-Contreras, E. A. Hayouni, C. E. Mays, C. Soto, I. Moreno-Gonzalez, *Cell. Mol. Life Sci.* **2018**, *75*, 3521–3538; b) P. Velander, L. Wu, F. Henderson, S. Zhang, D. R. Bevan, B. Xu, *Biochem. Pharmacol.* **2017**, *139*, 40–55.
[4] a) P. Cao, D. P. Raleigh, *Biochemistry* **2012**, *51*, 2670–2683; b) P. Velander, L. Wu, W. K. Ray, R. F. Helm, B. Xu, *Biochemistry* **2016**, *55*, 4255–4258; c) I. R. Sequeira, S. D. Poppitt, *Nutrients* **2017**, *9*, 788; d) A. A. Alkahtane, H. A. Alghamdi, B. Almutairi, M. M. Khan, M. S. Hasnain, M. M. Abdel-Daim, W. M. Alghamdi, S. Alkahtani, *Int. J. Med. Sci.* **2021**, *18*, 199–206.
[5] H. M. Awad, M. G. Boersma, S. Boeren, P. J. van Bladeren, J. Vervoort, I. M. Rietjens, *Chem. Res. Toxicol.* **2001**, *14*, 398–408.
[6] a) M. Zhu, S. Han, A. L. Fink, *Biochim. Biophys. Acta* **2013**, *1830*, 2872–2881; b) M. Zhu, S. Rajamani, J. Kaylor, S. Han, F. Zhou, A. L. Fink, *J. Biol. Chem.* **2004**, *279*, 26846–26857; c) T. Ginex, M. Trius, F. J. Luque, *Chem. Eur. J.* **2018**, *24*, 5813–5824.
[7] F. L. Palhano, J. Lee, N. P. Grimster, J. W. Kelly, *J. Am. Chem. Soc.* **2013**, *135*, 7503–7510.
[8] M. Sato, K. Murakami, M. Uno, Y. Nakagawa, S. Katayama, K. Akagi, Y. Masuda, K. Takegoshi, K. Irie, *J. Biol. Chem.* **2013**, *288*, 23212–23224.
[9] J. Sun, T. Murata, H. Shigemori, *J. Nat. Med.* **2020**, *74*, 579–583.
[10] E. O. Choi, J. W. Jeong, C. Park, S. H. Hong, G. Y. Kim, H. J. Hwang, E. J. Cho, Y. H. Choi, *Int. J. Mol. Med.* **2016**, *37*, 798–806.
[11] S. M. Choi, B. C. Kim, Y. H. Cho, K. H. Choi, J. Chang, M. S. Park, M. K. Kim, K. H. Cho, J. K. Kim, *Chonnam. Med. J.* **2014**, *50*, 45–51.
[12] S. Q. Zhang, D. Obregon, J. Ehrhart, J. Deng, J. Tian, H. Hou, B. Giunta, D. Sawmiller, J. Tan, *J. Neurosci. Res.* **2013**, *91*, 1239–1246.
[13] R. Malisauskas, A. Botyriute, J. G. Cannon, V. Smirnovas, *PLoS One* **2015**, *10*, e0121231.
[14] R. Lantz, B. Busbee, E. P. Wojcikiewicz, D. Du, *Chem. Eur. J.* **2020**, *26*, 13063–13071.
[15] a) K. Hashida, R. Makino, S. Ohara, *Holzforschung* **2009**, *63*, 319–326; b) F. J. Wang, J. Y. Bae, A. R. Jacobson, Y. H. Lee, L. M. Sayre, *J. Org. Chem.* **1994**, *59*, 2409–2417.
[16] a) Y. Q. Ding, Y. Z. Cui, T. D. Li, *J. Phys. Chem. A* **2015**, *119*, 4252–4260; b) B. Vilanova, J. M. Gallardo, C. Caldes, M. Adrover, J. Ortega-Castro, F. Munoz, J. Donoso, *J. Phys. Chem. A* **2012**, *116*, 1897–1905; c) C. Solis-Calero, J. Ortega-Castro, A. Hernandez-Laguna, F. Munoz, *Theor. Chem. Acc.* **2012**, *131*, 1263; d) M. Largeron, A. Neudorffer, M. B. Fleury, *J. Chem. Soc. Perkin Trans. 2* **1998**, 2721–2727.
[17] N. E. Hall, B. J. Smith, *J. Phys. Chem. A* **1998**, *102*, 4930–4938.
[18] S. Sinha, D. H. Lopes, Z. Du, E. S. Pang, A. Shanmugam, A. Lomakin, P. Talbiersky, A. Tennstaedt, K. McDaniel, R. Bakshi, P. Y. Kuo, M. Ehrmann, G. B. Benedek, J. A. Loo, F. G. Klarner, T. Schrader, C. Wang, G. Bitan, *J. Am. Chem. Soc.* **2011**, *133*, 16958–16969.
[19] a) M. H. Wu, A. C. Chan, L. H. Tu, *Biochimie* **2020**, *177*, 153–163; b) Y. H. Hsu, Y. W. Chen, M. H. Wu, L. H. Tu, *Biophys. J.* **2019**, *116*, 2304–2313.
[20] A. D. Becke, *J. Chem. Phys.* **1993**, *98*, 5648–5652.
[21] S. Grimme, J. Antony, S. Ehrlich, H. Krieg, *J. Chem. Phys.* **2010**, *132*, 154104.
[22] P. C. Harihara, J. A. Pople, *Theor. Chim. Acta* **1973**, *28*, 213–222.
[23] A. V. Marenich, C. J. Cramer, D. G. Truhlar, *J. Phys. Chem. B* **2009**, *113*, 6378–6396.
[24] A. E. Reed, R. B. Weinstock, F. Weinhold, *J. Chem. Phys.* **1985**, *83*, 735–746.
[25] Z. Jia, T. Ramstad, M. Zhong, *Electrophoresis* **2001**, *22*, 1112–1118.
[26] a) D. S. Kristol, P. Krautheim, S. Stanley, R. C. Parker, *Bioorg. Chem.* **1975**, *4*, 299–304; b) I. Andre, S. Linse, F. A. Mulder, *J. Am. Chem. Soc.* **2007**, *129*, 15805–15813.
[27] a) N. F. Bras, M. A. Perez, P. A. Fernandes, P. J. Silva, M. J. Ramos, *J. Chem. Theory Comput.* **2011**, *7*, 3898–3908; b) P. Georgieva, F. Himo, *J. Comput. Chem.* **2010**, *31*, 1707–1714.
[28] N. F. Bras, P. A. Fernandes, M. J. Ramos, S. D. Schwartz, *Chem. Eur. J.* **2018**, *24*, 1978–1987.
[29] T. H. Dunning, *J. Chem. Phys.* **1989**, *90*, 1007–1023.
[30] M. J. Frisch, G. W. Trucks, H. B. Schlegel, G. E. Scuseria, M. A. Robb, J. R. Cheeseman, G. Scalmani, V. Barone, G. A. Petersson, H. Nakatsuji, X. Li,

M. Caricato, A. Marenich, J. Bloino, B. G. Janesko, R. Gomperts, B. Mennucci, H. P. Hratchian, J. V. Ortiz, A. F. Izmaylov, J. L. Sonnenberg, D. Williams-Young, F. Ding, F. Lipparini, F. Egidi, J. Goings, B. Peng, A. Petrone, T. Henderson, D. Ranasinghe, V. G. Zakrzewski, J. Gao, N. Rega, G. Zheng, W. Liang, M. Hada, M. Ehara, K. Toyota, R. Fukuda, J. Hasegawa, M. Ishida, T. Nakajima, Y. Honda, O. Kitao, H. Nakai, T. Vreven, K. Throssell, J. A. Montgomery, Jr., J. E. Peralta, F. Ogliaro, M. Bearpark, J. J. Heyd, E. Brothers, K. N. Kudin, V. N. Staroverov, T. Keith, R. Kobayashi, J. Normand, K. Raghavachari, A. Rendell, J. C. Burant, S. S. Iyengar, J. Tomasi, M. Cossi, J. M. Millam, M. Klene, C. Adamo, R. Cammi, J. W. Ochterski, R. L. Martin, K. Morokuma, O. Farkas, J. B. Foresman, D. J. Fox, *Gaussian v.09*, Gaussian, Inc., Wallingford CT, **2016**.

[31] F. Neese, F. Wennmohs, U. Becker, C. Riplinger, *J. Chem. Phys.* **2020**, *152*, 224108.

[32] a) N. L. Haworth, Q. Wang, M. L. Coote, *J. Phys. Chem. A* **2017**, *121*, 5217–5225; b) P. G. Seybold, G. C. Shields, *Wiley Interdiscip. Rev.: Comput. Mol. Sci.* **2015**, *5*, 290–297.

[33] a) M. Wolniak, J. Oszmianski, I. Wawer, *Magn. Reson. Chem.* **2008**, *46*, 215–225; b) Z. S. Markovic, J. M. Dimitric Markovic, D. Milenkovic, N. Filipovic, *J. Mol. Model.* **2011**, *17*, 2575–2584.

[34] M. Rossi, R. Meyer, P. Constantinou, F. Caruso, D. Castelbuono, M. O'Brien, V. Narasimhan, *J. Nat. Prod.* **2001**, *64*, 26–31.

[35] M. R. Fesen, Y. Pommier, F. Leteurtre, S. Hiroguchi, J. Yung, K. W. Kohn, *Biochem. Pharmacol.* **1994**, *48*, 595–608.

[36] M. Musialik, R. Kuzmicz, T. S. Pawlowski, G. Litwinienko, *J. Org. Chem.* **2009**, *74*, 2699–2709.

[37] R. Alvarez-Diduk, M. T. Ramirez-Silva, A. Galano, A. Merkoci, *J. Phys. Chem. B* **2013**, *117*, 12347–12359.

[38] Y. Lee, H. Yeo, S. H. Liu, Z. Jiang, R. M. Savizky, D. J. Austin, Y. C. Cheng, *J. Med. Chem.* **2004**, *47*, 5555–5566.

[39] a) T. Mizutani, H. Takagi, U. Yoshiyuki, T. Horiguchi, K. Yamamura, H. Ogoshi, *J. Phys. Org. Chem.* **1998**, *11*, 737–742; b) J. E. Barry, M. Finkelstein, S. D. Ross, *J. Org. Chem.* **1984**, *49*, 1669–1671.

[40] F. J. Santiago-Medina, A. Pizzi, M. C. Basso, L. Delmotte, A. Celzard, *Polymer* **2017**, *9*, 37.

[41] a) D. Wozniak, A. Drys, A. Matkowski, *Nat. Prod. Res.* **2015**, *29*, 1567–1570; b) Y. K. Han, H. Kim, H. Shin, J. Song, M. K. Lee, B. Park, K. Y. Lee, *Molecules* **2020**, *25*, 3617; c) Z. Gao, K. Huang, X. Yang, H. Xu, *Biochim. Biophys. Acta* **1999**, *1472*, 643–650.

[42] C. Tang, J. Tan, J. Jin, S. Xi, H. Li, Q. Xie, X. Peng, *Rapid Commun. Mass Spectrom.* **2015**, *29*, 1863–1873.

[43] Z. Feng, J. Zhou, X. Shang, G. Kuang, J. Han, L. Lu, L. Zhang, *Pharm. Biol.* **2017**, *55*, 1177–1184.

[44] A. T. Garrison, Y. Abouelhassan, D. Kallifidas, F. Bai, M. Ukhanova, V. Mai, S. Jin, H. Luesch, R. W. Huigens 3rd, *Angew. Chem. Int. Ed.* **2015**, *54*, 14819–14823; *Angew. Chem.* **2015**, 127, 15032–15036.

[45] S. Morimoto, N. Tateishi, T. Matsuda, H. Tanaka, F. Taura, N. Furuya, N. Matsuyama, Y. Shoyama, *J. Biol. Chem.* **1998**, *273*, 12606–12611.

[46] C. A. Perez, Y. Wei, M. Guo, *J. Inorg. Biochem.* **2009**, *103*, 326–332.

[47] Y. H. Lee, Y. Lin, S. J. Cox, M. Kinoshita, B. R. Sahoo, M. Ivanova, A. Ramamoorthy, *Biochim. Biophys. Acta Proteins Proteomics* **2019**, *1867*, 529–536.

[48] Z. X. Xu, Q. Zhang, G. L. Ma, C. H. Chen, Y. M. He, L. H. Xu, Y. Zhang, G. R. Zhou, Z. H. Li, H. J. Yang, P. Zhou, *J. Diabetes Res.* **2016**, *2016*, 1867059.

[49] G. Grasso, H. Komatsu, P. H. Axelsen, *J. Inorg. Biochem.* **2017**, *174*, 130–136.

[50] H. S. Fernandes, M. J. Ramos, N. M. F. S. A. Cerqueira, *Chem. Eur. J.* **2017**, *23*, 9162–9173.

[51] W. Li, J. Pi, Y. Zhang, X. Ma, B. Zhang, S. Wang, D. Qi, N. Li, P. Guo, Z. Liu, *Fitoterapia* **2018**, *129*, 85–93.

[52] S. Gautam, S. Karmakar, R. Batra, P. Sharma, P. Pradhan, J. Singh, B. Kundu, P. K. Chowdhury, *Biochim. Biophys. Acta Proteins Proteomics* **2017**, *1865*, 589–603.

Manuscript received: November 26, 2021
Accepted manuscript online: January 6, 2022
Version of record online: January 27, 2022